

# Iterative coordinates

Chongyang Deng · Qingjun Chang · Kai Hormann

---

## Abstract

Barycentric coordinates provide a simple way of expressing the linear interpolant to data given at the vertices of a triangle and have numerous applications in computer graphics and other fields. The generalization of barycentric coordinates to polygons with more than three vertices is not unique and many constructions have been proposed. Among them, mean value coordinates stand out by having a simple closed form and being well-defined for arbitrary polygons, but they may take on large negative values in the case of concave polygons, leading to artefacts in applications like shape deformation. We present a modification of mean value coordinates that is based on the observation that the mean value coordinates of some point  $v$  inside a polygon can be negative if the central projection of the polygon onto the unit circle around  $v$  folds over. By iteratively smoothing the projected polygon and carrying over this smoothing procedure to the barycentric coordinates of  $v$ , these fold-overs as well as the negative coordinate values and shape deformation artefacts gradually disappear, and they are guaranteed to completely vanish after a finite number of iterations.

## Citation Info

*Journal*  
Computer Aided Geometric Design  
*Volume*  
79, May 2020  
*Article*  
101861, 13 pages  
*Note*  
Proceedings of GMP  
*DOI*  
[10.1016/j.cagd.2020.101861](https://doi.org/10.1016/j.cagd.2020.101861)

---

## 1 Introduction

Möbius [24] observed that any point  $v$  in the plane can be written as a unique affine combination of the vertices of a triangle  $T$ , and he called the weights of this affine combination the *barycentric coordinates* of  $v$  with respect to  $T$ . Barycentric coordinates are widely used in computer graphics for interpolating vertex attributes such as colours, normals, or texture coordinates over the triangles of a triangle mesh, and they also play a key role in other disciplines. Over the last two decades, barycentric coordinates have been generalized to arbitrary polygons and polytopes, which has led to novel solutions in applications like mesh parameterization [7], image warping [28], shape deformation [16], generalized Bézier surfaces [20], finite element methods [10], and many more [14].

All these applications have in common that they require to interpolate data  $f_1, \dots, f_n \in \mathbb{R}^m$  given at the vertices  $v_1, \dots, v_n$  of a polytope  $\Omega \subset \mathbb{R}^d$  with  $n \geq d + 1$ , and they benefit from the *barycentric interpolant*

$$f: \Omega \rightarrow \mathbb{R}^m, \quad f(v) = \sum_{i=1}^n \lambda_i(v) f_i, \quad (1)$$

where the functions  $\lambda_i: \Omega \rightarrow \mathbb{R}$ ,  $i = 1, \dots, n$  are *generalized barycentric coordinates* with most or even all of the following properties:

- *Partition of unity*:  $\sum_{i=1}^n \lambda_i(v) = 1$  for  $v \in \Omega$ ;
- *Linear reproduction*:  $\sum_{i=1}^n \lambda_i(v) v_i = v$  for  $v \in \Omega$ ;
- *Lagrange property*:  $\lambda_i(v_j) = \delta_{i,j}$  for  $i, j = 1, \dots, n$ ;
- *Non-negativity*:  $\lambda_i(v) \geq 0$  for  $v \in \Omega$  and  $i = 1, \dots, n$ ;
- *Smoothness*:  $\lambda_1(v), \dots, \lambda_n(v)$  vary smoothly with  $v \in \Omega$ ;
- *Linearity on the edges*:  $\lambda_i$  is linear on the edges of  $\Omega$ .

The Lagrange property ensures that  $f$  in (1) is indeed an interpolant of the given data, and the linear reproduction property guarantees that linear functions, including the identity, are reproduced, which is crucial for shape deformation. Non-negativity and partition of unity imply that the interpolated values  $f(v)$  are inside the convex hull of the data, and smoothness usually refers to  $C^1$  or  $C^2$  continuity, which is important if derivatives of  $f$  are needed. Linearity on the edges is not a strict requirement, but, like the Lagrange property, a consequence of the other properties in the case of convex polytopes [9, 3].

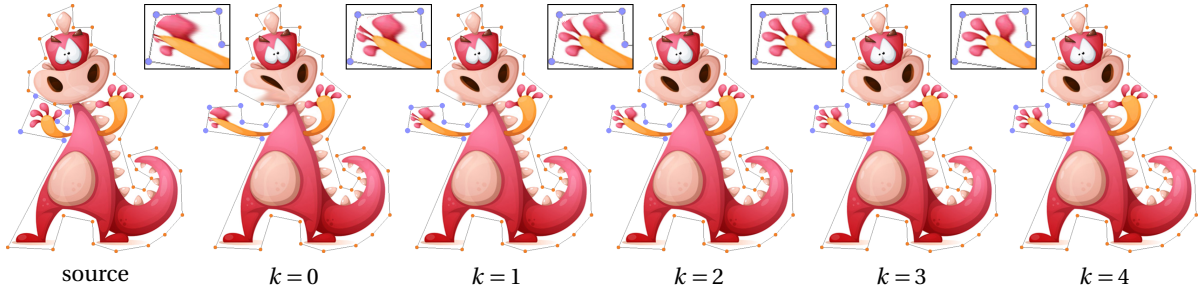


**Figure 1:** Deformation of a source image (left), obtained by moving six vertices (blue) of the control polygon. The deformation based on mean value coordinates ( $k = 0$ ) exhibits severe artefacts, caused by negative coordinate values. Using iterative coordinates, these deformation artefacts gradually disappear as the number of iterations increases ( $k = 1, 2, 3, 4$ ).

## 1.1 Related work

While barycentric coordinates are unique for simplices, several constructions have been proposed for arbitrary polygons and polytopes. Kalman [17] was probably the first to generalize barycentric coordinates to convex polyhedra, but his coordinates are only  $C^0$ . Using projective geometry, Wachspress [26] later derived smooth and rational coordinates for convex polygons, which have a simple closed form [23] and can be extended to higher dimensions [27]. However, these *Wachspress coordinates*, as well as *discrete harmonic coordinates* [5], are not well-defined for concave polygons.

Floater [8] was the first to discover a simple closed-form construction of smooth coordinates that are well-defined for arbitrary polygons [12], but these *mean value coordinates* can be negative for concave polygons. The same holds for *metric* [21], *Poisson* [18], and *Gordon–Wixom coordinates* [2]. Instead, *positive mean value* [19], *positive Gordon–Wixom* [22], and *power coordinates* [3] are positive inside arbitrary polygons, but not smooth. *Blended barycentric coordinates* [1] overcome this limitation, but they depend on an initial triangulation of  $\Omega$ .

The only known coordinates that are non-negative for arbitrary polygons and polyhedra and at least  $C^1$  are *harmonic* [15], *maximum entropy* [13], and *local barycentric coordinates* [29, 25], but they do not have a closed form and can only be approximated numerically.

## 1.2 Contributions

In this paper we propose a simple, iterative modification of planar mean value coordinates that effectively reduces negative coordinate values and related deformation artefacts after few iterations (see Figure 1). Like mean value coordinates, these *iterative coordinates* are smooth ( $C^\infty$ ), provided that the same number of iterations is used for all domain points, and they are guaranteed to be non-negative after a finite number of iterations. While iterative coordinates do not have a simple closed form, they can be evaluated exactly at any point  $v \in \Omega$  with a simple and efficient algorithm (Section 5). After providing some preliminaries and introducing a novel representation of mean value coordinates in terms of *circumcentre coordinates* (Section 2), we describe the construction of iterative coordinates for arbitrary polygons (Section 3), prove their properties (Section 4), and discuss their limitations and possible directions for future work (Section 6).

## 2 Background

Let  $\Omega$  be a simple planar polygon with  $n$  vertices  $v_1, \dots, v_n \in \mathbb{R}^2$ . Without loss of generality, we assume that the vertices are given in counterclockwise order. We further consider indices periodically over the range  $1, \dots, n$  and hence identify the index  $n + 1$  with 1 and the index 0 with  $n$ .

### 2.1 Three-point coordinates

If  $\Omega$  is a *convex* polygon, then Floater, Hormann, and Kós [9] show that the functions  $w_{i,p}: \text{int}(\Omega) \rightarrow \mathbb{R}$  for  $i = 1, \dots, n$  with

$$w_{i,p}(v) = \frac{r_{i+1}(v)^p A_{i-1}(v) - r_i(v)^p B_i(v) + r_{i-1}(v)^p A_i(v)}{A_{i-1}(v)A_i(v)}, \quad (2)$$

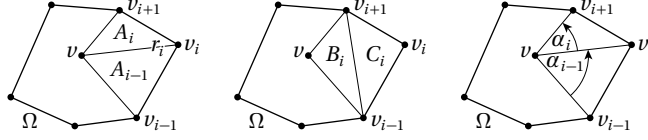


**Figure 2:** Notation of distances, areas, and signed angles.

where  $r_i(v) = \|v_i - v\|$  and  $A_i(v)$  and  $B_i(v)$  are the *signed* areas of the triangles  $[v, v_i, v_{i+1}]$  and  $[v, v_{i-1}, v_i]$ , respectively (see Figure 2), are *homogeneous coordinates* of  $v$  with respect to  $\Omega$ , that is, they satisfy

$$\sum_{i=1}^n w_{i,p}(v)(v_i - v) = 0$$

for any  $p \in \mathbb{R}$ . They call them *three-point coordinates*, because each  $w_{i,p}$  depends only on  $v_{i-1}$ ,  $v_i$ , and  $v_{i+1}$ , and they prove that Wachspress, mean value, and discrete harmonic coordinates are special cases of the *normalized* three-point coordinates

$$\lambda_{i,p} = \frac{w_{i,p}}{\sum_{j=1}^n w_{j,p}}, \quad i = 1, \dots, n,$$

for  $p = 0$ ,  $p = 1$ , and  $p = 2$ , respectively.

## 2.2 Cyclic polygons

Floater, Hormann, and Kós [9] also show that Wachspress and discrete harmonic coordinates are identical for any  $v$  inside a convex *cyclic* polygon  $\Omega$  with radius  $R$ . We further conclude from (2) that *all* normalized three-point coordinates are identical at the circumcentre  $\hat{v}$  of  $\Omega$ , because the common factor  $R^p = r_i^p$  for  $i = 1, \dots, n$  in the numerators of the homogeneous coordinates  $w_{i,p}$  cancels out in the normalization. As three-point coordinates are invariant to similarities, we can assume  $R = 1$ , so that (2) simplifies to

$$\hat{w}_i = \frac{A_{i-1} - B_i + A_i}{A_{i-1}A_i} = \frac{C_i}{A_{i-1}A_i}, \quad i = 1, \dots, n, \quad (3)$$

where  $C_i$  is the *signed* area of the triangle  $[v_{i-1}, v_i, v_{i+1}]$  (see Figure 2). Since  $\Omega$  is convex, these  $\hat{w}_i$  are positive, and we call them the *circumcentre coordinates* of the cyclic polygon  $\Omega$ .

**Remark 1.** The  $\hat{w}_i$  in (3) are homogeneous coordinates of the circumcentre  $\hat{v}$ , even if  $\Omega$  is self-intersecting or if  $\hat{v}$  lies outside  $\Omega$ , but they are not necessarily positive in either case.

## 2.3 Mean value coordinates

The mean value coordinates  $\lambda_{i,1}$  are the only three-point coordinates that extend to *concave* polygons, and they can also be defined via normalization of the homogeneous coordinates

$$\hat{w}_i = \frac{\tan(\alpha_{i-1}/2) + \tan(\alpha_i/2)}{r_i}, \quad i = 1, \dots, n, \quad (4)$$

where  $\alpha_i(v)$  denotes the *signed* angle in the triangle  $[v, v_i, v_{i+1}]$  at  $v$  (see Figure 2), because  $\hat{w}_i = w_{i,1}/2$  [9]. Besides these known definitions, we observe that mean value coordinates can alternatively be derived by considering the cyclic polygon  $\Omega'$  with vertices  $v'_i = v + (v_i - v)/r_i$ ,  $i = 1, \dots, n$ , that we get by projecting the vertices of  $\Omega$  onto the unit circle around  $v$ .

**Lemma 2.** *The mean value coordinates of  $v$  with respect to  $\Omega$  are equal to the scaled and normalized circumcentre coordinates of  $\Omega'$ ,*

$$\lambda_{i,1} = \frac{\hat{w}'_i/r_i}{\sum_{j=1}^n \hat{w}'_j/r_j}, \quad i = 1, \dots, n.$$

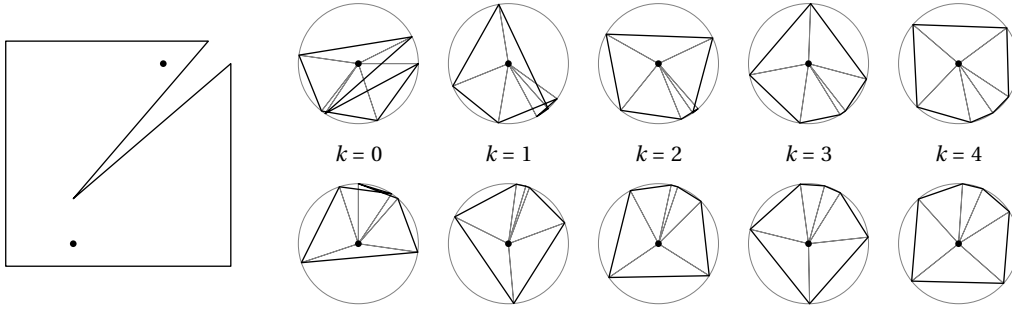


**Figure 3:** The main idea of iterative coordinates is to project the polygon  $\Omega$  (left) onto the unit circle around  $v$  ( $k = 0$ ) and then iteratively apply midpoint averaging plus rescaling to the vertices of the resulting cyclic polygon ( $k = 1, 2, \dots$ ). The top and bottom row illustrate the effect of this procedure for the two interior points of  $\Omega$  shown on the left.

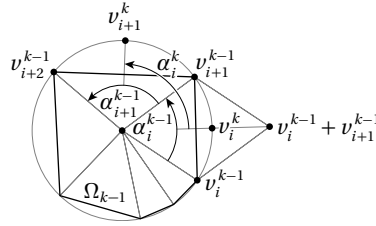


**Figure 4:** Notation of vertices and angles used for describing midpoint averaging plus rescaling.

*Proof.* The statement follows by first noticing that the projection does not change the angles around  $v$ , that is,  $\alpha'_i = \alpha_i$ , and then using simple trigonometry, as in [9], to find that

$$\hat{w}_i r_i = \tan \frac{\alpha_{i-1}}{2} + \tan \frac{\alpha_i}{2} = \tan \frac{\alpha'_{i-1}}{2} + \tan \frac{\alpha'_i}{2} = \frac{1}{2} \frac{C'_i}{A'_{i-1} A'_i} = \frac{\hat{w}'_i}{2}$$

for  $i = 1, \dots, n$ . □

### 3 Iterative coordinates

From Lemma 2 it is easy to deduce the known fact that mean value coordinates are positive for any  $v$  inside the kernel of  $\Omega$ , because  $\Omega'$  is convex in that case. Otherwise,  $\Omega'$  is self-intersecting, which may result in negative coordinates. To overcome this limitation, we propose to iteratively apply a simple smoothing operator to ‘untangle’ the projected polygon (see Figure 3).

#### 3.1 Construction

Let  $v \in \text{int}(\Omega)$  be any point from the interior of  $\Omega$ . In order to keep the formulas simple, we use the fact that homogeneous coordinates are invariant to translations and shift everything by  $-v$ , so that  $(0, 0)$  becomes the circumcentre. That is, we let  $\Omega_0$  be the cyclic polygon with vertices

$$v_i^0 = \frac{v_i - v}{r_i}, \quad i = 1, \dots, n, \quad (5)$$

and then compute cyclic polygons  $\Omega_k$  for  $k = 1, 2, \dots$ , with vertices  $v_i^k$  defined iteratively as

$$v_i^k = \frac{v_i^{k-1} + v_{i+1}^{k-1}}{s_i^k}, \quad s_i^k = \|v_i^{k-1} + v_{i+1}^{k-1}\|, \quad i = 1, \dots, n, \quad (6)$$

as shown in Figure 4. This smoothing process is quite effective at ‘untangling’  $\Omega_0$  (see Figure 3), and we will prove below that it yields a convex cyclic polygon  $\Omega_k$  after a finite number of iterations (see Section 4). But before going into technical details, let us first explain how to use this approach for deriving novel generalized barycentric coordinates of  $v$  with respect to  $\Omega$ .

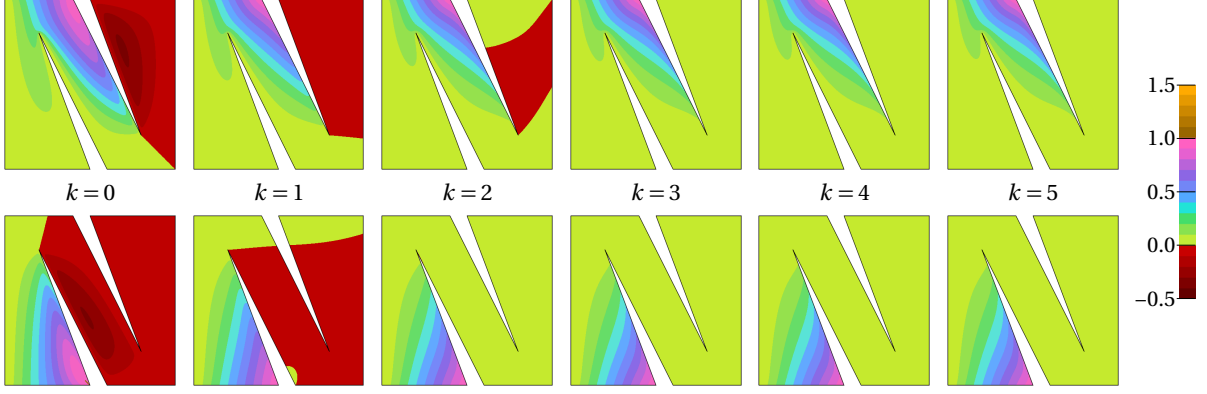


**Figure 5:** Comparison of iterative coordinates for different values of  $k$  for a concave polygon.

To this end, let  $V_k = (v_1^k, \dots, v_n^k)$  be the  $2 \times n$  matrices that contain the vertices of  $\Omega_k$  as columns, and likewise  $V = (v_1, \dots, v_n)$  for the given polygon  $\Omega$ . We can then express the initial projection in (5) and the recurrence relation in (6) as

$$V_0 = (V - \nu \mathbf{e}^\top) S_0, \quad V_k = V_{k-1} M S_k, \quad k \in \mathbb{N}, \quad (7)$$

where

$$\mathbf{e} = \begin{pmatrix} 1 \\ 1 \\ \vdots \\ 1 \\ 1 \\ 1 \end{pmatrix}, \quad S_0 = \text{diag}\left(\frac{1}{r_1}, \dots, \frac{1}{r_n}\right), \quad S_k = \text{diag}\left(\frac{1}{s_1^k}, \dots, \frac{1}{s_n^k}\right), \quad M = \begin{pmatrix} 1 & 0 & \cdots & 0 & 1 \\ 1 & 1 & \cdots & 0 & 0 \\ \vdots & \ddots & \ddots & \vdots & \vdots \\ 0 & \cdots & 1 & 1 & 0 \\ 0 & \cdots & 0 & 1 & 1 \end{pmatrix}. \quad (8)$$

It follows that

$$V_k = (V - \nu \mathbf{e}^\top) T_k, \quad k \in \mathbb{N}_0,$$

where the matrices  $T_k$  are defined recursively as

$$T_0 = S_0, \quad T_k = T_{k-1} M S_k, \quad k \in \mathbb{N}. \quad (9)$$

Denoting the circumcentre coordinates of  $\Omega_k$  by  $\hat{\mathbf{w}}_k = (\hat{w}_1^k, \dots, \hat{w}_n^k)^\top$ , we find that

$$\mathbf{w}_k = (w_1^k, \dots, w_n^k)^\top = T_k \hat{\mathbf{w}}_k \quad (10)$$

are homogeneous coordinates of  $\nu$  with respect to  $\Omega$ , because

$$\sum_{i=1}^n w_i^k (v_i - \nu) = (V - \nu \mathbf{e}^\top) \mathbf{w}_k = V_k \hat{\mathbf{w}}_k = \sum_{i=1}^n \hat{w}_i^k v_i^k = 0. \quad (11)$$

**Definition 3.** For any  $k \in \mathbb{N}_0$ , the *iterative coordinates*  $\lambda_i^k: \Omega \rightarrow \mathbb{R}$ ,  $i = 1, \dots, n$  are defined as

$$\lambda_i^k = \frac{w_i^k}{\sum_{j=1}^n w_j^k}, \quad i = 1, \dots, n. \quad (12)$$

By Lemma 2, it is clear that iterative coordinates include mean value coordinates as the special case  $k = 0$ .

### 3.2 Examples

Figure 5 shows the effect that the smoothing iterations have on the corresponding barycentric coordinates in the case of concave polygons. While mean value coordinates ( $k = 0$ ) may have rather large negative values, especially close to edges adjacent to concave corners, a small number of iterations usually suffices to reduce the magnitude of these negative values considerably. As  $k$  grows, the coordinate functions eventually

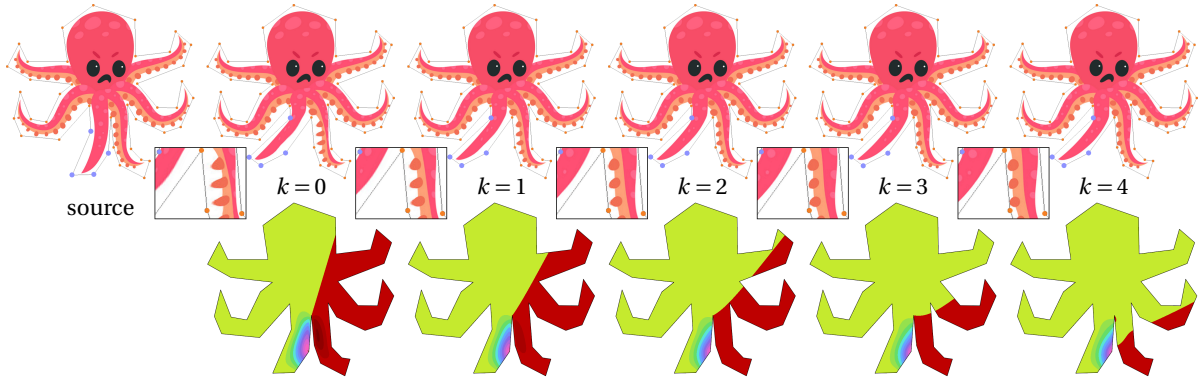


**Figure 6:** Deformation of a source image (left), obtained by moving four vertices (blue) of the control polygon, using iterative coordinates with respect to the source control polygon (top row). The deformation artefacts (close-ups) are caused by the negative values (red) of the indicated coordinate function (bottom row), which are relatively large for mean value coordinates ( $k = 0$ ), but quickly become negligible as the number of iterations increases ( $k = 1, 2, 3, 4$ ). Function values are visualized using the colour bar in Figure 5.

become non-negative (see Section 4), and further increasing the number of iterations has a marginal effect on the shape of the coordinate functions.

Figure 6 illustrates the impact that this behaviour has in the context of shape deformation. Large negative coordinate values can lead to severe deformation artefacts if the corresponding control polygon vertex is moved, because they induce a significant shift in the opposite direction. As  $k$  increases, the effect of negative values quickly becomes negligible and these artefacts disappear, even before the coordinate function becomes non-negative. For example, the coordinate function shown in Figure 6 is completely non-negative only for  $k \geq 7$ , but the deformation artefact disappears already for  $k = 4$ , when the function is still slightly negative in the red region with a smallest function value of about  $-0.0168388$ .

## 4 Properties

One of the key properties of iterative coordinates is that they are guaranteed to be non-negative after a finite number of iterations. To prove this claim, let us first analyse what happens to the cyclic polygons  $\Omega_k$  in the limit, as  $k$  approaches infinity.

**Lemma 4.** *The sequence  $(\Omega_k)_{k \in \mathbb{N}_0}$  of cyclic polygons defined in Section 3.1 converges to a regular polygon.*

*Proof.* The iterative procedure in (6) for computing  $\Omega_k$  from  $\Omega_{k-1}$  for  $k \in \mathbb{N}$  implies (see Figure 4) that the signed angles  $\alpha_i^k = \sphericalangle(v_i^k, v_{i+1}^k)$  satisfy the recurrence relation

$$\alpha_i^k = \frac{\alpha_i^{k-1} + \alpha_{i+1}^{k-1}}{2}, \quad i = 1, \dots, n. \quad (13)$$

Gathering all angles in the vector  $\mathbf{\alpha}_k = (\alpha_1^k, \dots, \alpha_n^k)^\top \in \mathbb{R}^n$ , this relation can be expressed as

$$\mathbf{\alpha}_k = A\mathbf{\alpha}_{k-1} = A^2\mathbf{\alpha}_{k-2} = \dots = A^k\mathbf{\alpha}_0, \quad k \in \mathbb{N},$$

where  $A = M^\top/2$  with  $M$  defined as in (8). As  $A$  is a circulant matrix, it is well known [4] that the eigenvectors of  $A$  are orthogonal and that  $\mu_0 = 1$  is the unique dominant eigenvalue of  $A$  with normalized eigenvector  $\mathbf{e}_0 = \mathbf{e}/\sqrt{n}$ . Therefore, as shown in [6],

$$\lim_{k \rightarrow \infty} \mathbf{\alpha}_k = (\mathbf{e}_0^\top \mathbf{\alpha}_0) \mathbf{e}_0 = \frac{\alpha_1^0 + \dots + \alpha_n^0}{\sqrt{n}} \mathbf{e}_0 = \left( \frac{2\pi}{n}, \dots, \frac{2\pi}{n} \right)^\top,$$

which means that the limit polygon is regular.  $\square$

Lemma 4 implies that all  $\alpha_i^k$  are positive and hence  $\Omega_k$  is convex if  $k$  is large enough, which in turn means that the iterative coordinates  $\lambda_i^k$  are also positive.

**Corollary 5.** *The iterative coordinates  $\lambda_i^k$  in (12) are positive over  $\text{int}(\Omega)$  for  $k$  sufficiently large.*

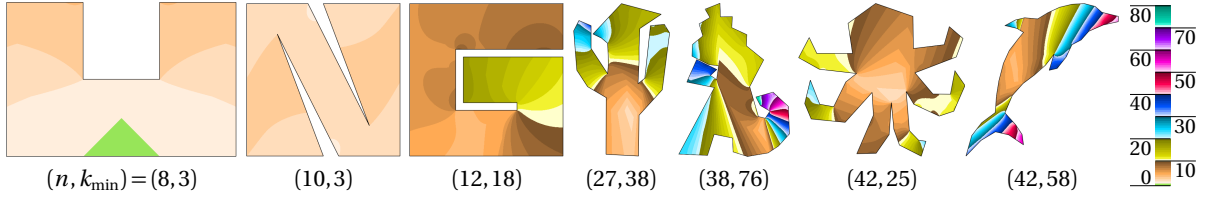


**Figure 7:** Examples of concave polygons with different numbers of  $n$  vertices, for which the iterative coordinates are non-negative after the stated number of  $k_{\min}$  iterations (determined by regularly sampling the polygon's bounding square and computing the coordinates for the interior sample points in double precision at a resolution of  $10^3 \times 10^3$  for the whole square and an effective resolution of  $10^6 \times 10^6$  in the regions where the largest number of iterations is needed). The colour-coding refers to the number of iterations required to get positive coordinates at the individual interior points.

*Proof.* By (3), the circumcentre coordinates  $\hat{w}_k$  of  $\Omega_k$  are positive if  $\Omega_k$  is convex. Since it follows from (9) and by induction over  $k$  that  $T_k$  is a non-negative matrix with strictly positive diagonal entries for any  $k \in \mathbb{N}_0$ , we conclude that the homogeneous coordinates  $w_k = T_k \hat{w}_k$  of  $v$  are positive, too, and so are the iterative coordinates  $\lambda_i^k$ .  $\square$

Clearly, the smallest number of iterations  $k$  for which the iterative coordinates  $\lambda_i^k(v)$  at some  $v \in \text{int}(\Omega)$  are positive depends on  $v$ , as shown in Figure 7, and the largest number of iterations is typically required in the extremities of a shape, like the tail and nose of the dolphin, as the fold-overs of the projected cyclic polygon  $\Omega_0$  are the worst for points in these regions.

Let us now derive a lower bound for the number of iterations, such that the iterative coordinates for *all* interior points of  $\Omega$  are positive.

**Theorem 6.** *If*

$$k \geq \frac{2}{\pi^2} n^2 \log(n+1), \quad (14)$$

then  $\alpha_i^k > 0$  for  $i = 1, \dots, n$ .

*Proof.* Let  $i \in \mathbb{C}$  be the imaginary unit and  $\omega = \exp(2\pi i/n) \in \mathbb{C}$  be an  $n$ -th root of unity. Then it is well known [4] that

$$\mu_j = \frac{1 + \omega^j}{2} = \omega^{j/2} \cos \frac{j\pi}{n} \in \mathbb{C}, \quad j = 0, \dots, n-1 \quad (15)$$

are the eigenvalues of  $A = M^T/2$ , where  $M$  is defined as in (8), with normalized eigenvectors

$$e_j = (1, \omega^j, \omega^{2j}, \dots, \omega^{(n-1)j})^T / \sqrt{n} \in \mathbb{C}^n, \quad j = 0, \dots, n-1.$$

Representing  $\alpha_0$  with respect to these orthonormal eigenvectors as  $\alpha_0 = \sum_{j=0}^{n-1} c_j e_j$  with coefficients

$$c_j = e_j^H \alpha_0 = \frac{1}{\sqrt{n}} \sum_{l=0}^{n-1} \omega^{-jl} \alpha_{l+1}^0, \quad j = 0, \dots, n, \quad (16)$$

we have  $\alpha_k = \sum_{j=0}^{n-1} c_j \mu_j^k e_j$  and can write the elements of  $\alpha_k$  as

$$\alpha_{i+1}^k = \frac{1}{\sqrt{n}} \sum_{j=0}^{n-1} c_j \mu_j^k \omega^{ij}, \quad i = 0, \dots, n-1.$$

Splitting off the first term and using the symmetry  $\mu_j = \overline{\mu_{n-j}}$  for  $j = 1, \dots, n-1$  as well as (15) and (16), we get

$$\begin{aligned} \alpha_{i+1}^k &= \frac{2\pi}{n} + \frac{1}{n} \sum_{j=1}^{n-1} \mu_j^k \sum_{l=0}^{n-1} \omega^{j(i-l)} \alpha_{l+1}^0 \\ &= \frac{2\pi}{n} + \frac{1}{n} \sum_{j=1}^{n'} \cos^k \frac{j\pi}{n} \sum_{l=0}^{n-1} (\omega^{jk/2} \omega^{j(i-l)} + \omega^{-jk/2} \omega^{(n-j)(i-l)}) \alpha_{l+1}^0 \\ &= \frac{2\pi}{n} + \frac{1}{n} \sum_{j=1}^{n'} \cos^k \frac{j\pi}{n} \sum_{l=0}^{n-1} 2 \cos \frac{2j(i-l+k/2)\pi}{n} \alpha_{l+1}^0, \end{aligned}$$

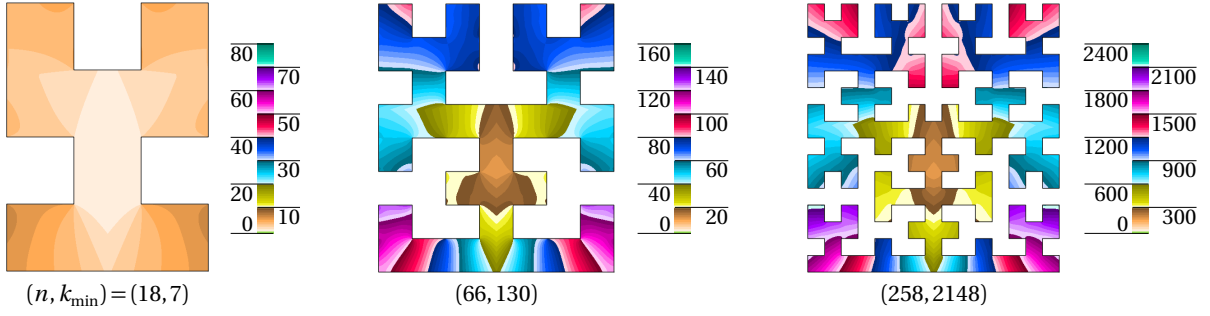


**Figure 8:** Number of iterations required to get positive coordinates at the individual interior points of the (closed) Hilbert curves  $H_2, H_3, H_4$  (from left to right); cf. Figure 7.

where  $n' = \lfloor (n-1)/2 \rfloor$ , and further

$$\alpha_{i+1}^k > \frac{2\pi}{n} - 2\pi \sum_{j=1}^{n'} \cos^k \frac{j\pi}{n}, \quad i=0, \dots, n-1, \quad (17)$$

because  $\cos x \in [-1, 1]$  for any  $x \in \mathbb{R}$  and  $\alpha_l^0 \in (-\pi, \pi)$  for  $l = 1, \dots, n$ . We now observe that the function  $f(x) = \log(\cos x) + x^2/2$  is negative for  $x \in (0, \pi/2)$ , because  $f(0) = 0$  and  $f'(x) = x - \tan x < 0$ , hence

$$\log\left(\cos \frac{\pi}{n}\right) < -\frac{(\pi/n)^2}{2}.$$

Applying exponentiation to both sides and using (14), we then have

$$\cos^k \frac{\pi}{n} < \exp\left(-\frac{k(\pi/n)^2}{2}\right) \leq \exp(-\log(n+1)) = \frac{1}{n+1}.$$

Recalling that  $\cos(2x) \leq \cos^4 x$  for any  $x \in \mathbb{R}$  and therefore

$$\cos \frac{j\pi}{n} \leq \cos \frac{2\pi}{n} \leq \cos^4 \frac{\pi}{n}, \quad j=2, \dots, n',$$

we finally conclude from (17) that

$$\alpha_i^k > \frac{2\pi}{n} - \frac{2\pi}{n+1} - \frac{n\pi}{(n+1)^4} > 0, \quad i=1, \dots, n. \quad \square$$

While the lower bound in (14) guarantees that the iterative coordinates for *any* polygon with  $n$  vertices are positive for *all* interior points of  $\Omega$ , Figure 7 shows that usually a much smaller number of  $k_{\min}$  iterations suffices. The reason for this is two-fold. On the one hand, the circumcentre coordinates  $\hat{w}_k$  of  $\Omega_k$  may be positive even if some of the angles  $\alpha_i^k$  are negative. More precisely,  $\hat{w}_i^k/2 = \tan(\alpha_{i-1}^k/2) + \tan(\alpha_i^k/2) > 0$ , if and only if  $\alpha_{i-1}^k + \alpha_i^k > 0$ . This explains the green triangle of points with non-negative mean value coordinates ( $k=0$ ) in the first example in Figure 7, even though these points do not belong to the kernel of this polygon, which is empty. On the other hand, the multiplication of  $\hat{w}_k$  with  $T_k$  to get  $w_k$  has another  $k$ -fold smoothing effect on the values  $\hat{w}_i^k$ , due to the matrix  $M$  that is contained  $k$  times in  $T_k$ .

However, there also exist examples where  $k_{\min}$  is rather large and presumably on the order of  $O(n^2)$ . Figure 8 shows examples of Hilbert curves of  $m$ -th order for  $m = 2, 3, 4$ . They are constructed by connecting the vertices of a regular  $2^m \times 2^m$  grid, following a recursive pattern (and allowing some vertices to be collinear with its neighbours), plus two extra vertices to get a closed polygon with  $n = 4^m + 2$  vertices. For these polygons, the number of iterations needed to get positive coordinates ranges from about  $n^2/360$  near the centre of the polygon to roughly  $n^2/36$  in the extremities close to the bottom left and bottom right. But even in these examples  $k_{\min}$  is still much smaller than the lower bound in Theorem 6.

We conclude this section by formally proving that iterative coordinates satisfy all the properties listed in Section 1.

**Theorem 7.** *The iterative coordinates  $\lambda_i^k$  in (12) are smooth and non-negative barycentric coordinates for  $k$  sufficiently large. They satisfy the Lagrange property and are linear along the edges of  $\Omega$ .*

*Proof.* We first remark that iterative coordinates are well-defined over the interior of  $\Omega$ . Indeed, if  $v \in \text{int}(\Omega)$ , then all vertices  $v_i^k$  in (5) and (6) are well-defined, because  $r_i > 0$  and  $\alpha_i = \alpha_i^0 \in (-\pi, \pi)$  for  $i = 1, \dots, n$ , so that  $\alpha_i^k \in (-\pi, \pi)$  by (13) and  $s_i^k > 0$  for  $i = 1, \dots, n$  and  $k \in \mathbb{N}$ . This further implies that the circumcentre coordinates  $\hat{w}_i^k = 2(\tan(\alpha_{i-1}^k/2) + \tan(\alpha_i^k/2))$ , the matrices  $T_k$ , and the homogeneous coordinates  $w_i^k$  are well-defined for  $i = 1, \dots, n$  and  $k \in \mathbb{N}_0$ . Moreover, if  $k$  is sufficiently large, then the  $w_i^k$  are positive and the  $\lambda_i^k$  well-defined for  $i = 1, \dots, n$ , because the denominator in (12) is positive, too.

The *partition of unity* and the *linear reproduction* properties then follow directly from the definition of  $\lambda_i^k$  in (12) and (11). Moreover, as a combination of sums, products, divisions, and compositions of analytic functions, the  $\lambda_i^k$  are analytic, too, and therefore *smooth* ( $C^\infty$ ).

To prove the *Lagrange property*, let  $\tilde{w}_k = (\tilde{w}_1^k, \dots, \tilde{w}_n^k)$  be the homogeneous iterative coordinates of  $(0, 0)$  with respect to  $\Omega_0$ . Then,  $\tilde{w}_k = \tilde{T}_k \hat{w}_k$ , as in (10), with  $\tilde{T}_0 = I$  and  $\tilde{T}_k = \tilde{T}_{k-1} M S_k$  for  $k \in \mathbb{N}$  as in (9), and  $w_k = S_0 \hat{w}_k$ , that is,  $w_i^k = \hat{w}_i^k / r_i$ . Now, as  $v$  approaches  $v_l$  for some fixed  $l \in \{1, \dots, n\}$ , the distances  $r_i = \|v_i - v\|$  converge to  $\|v_i - v_l\|$  and the  $\tilde{w}_i^k$  remain finite. Therefore,

$$\lim_{v \rightarrow v_l} (w_i^k r_l) = \lim_{v \rightarrow v_l} (\tilde{w}_i^k r_l / r_i) = \tilde{w}_i^k \delta_{i,l}$$

and consequently

$$\lim_{v \rightarrow v_l} \lambda_i^k = \lim_{v \rightarrow v_l} \left( w_i^k r_l / \sum_{j=1}^n w_j^k r_l \right) = \delta_{i,l}, \quad i = 1, \dots, n.$$

In other words, the Lagrange property is essentially a consequence of the initial projection in (5).

To handle the case when  $v$  approaches  $\bar{v} = (1 - \mu)v_l + \mu v_{l+1}$  for some fixed  $l \in \{1, \dots, n\}$  and  $\mu \in (0, 1)$ , we let  $\tilde{t}_{i,j}^k = \bar{s} t_{i,j}^k$  for  $i, j = 1, \dots, n$  and  $k \in \mathbb{N}_0$ , where  $t_{i,j}^k$  is the  $(i, j)$ -th entry of  $T_k$  and  $\bar{s} = s_l^1 = \|v_l^0 + v_{l+1}^0\|$ . Then,  $\lim_{v \rightarrow \bar{v}} \bar{s} = 0$ , and it follows from (9) that

$$\lim_{v \rightarrow \bar{v}} \tilde{t}_{i,j}^1 = \begin{cases} 1/r_l(\bar{v}), & \text{if } i = l \text{ and } j = l, \\ 1/r_{l+1}(\bar{v}), & \text{if } i = l+1 \text{ and } j = l, \\ 0, & \text{otherwise.} \end{cases}$$

More generally, we conclude by induction over  $k$  that

$$\lim_{v \rightarrow \bar{v}} \tilde{t}_{i,j}^k = 0, \quad i \neq l, l+1, \quad j = 1, \dots, n$$

and

$$r_l(\bar{v}) \lim_{v \rightarrow \bar{v}} \tilde{t}_{l,j}^k = r_{l+1}(\bar{v}) \lim_{v \rightarrow \bar{v}} \tilde{t}_{l+1,j}^k, \quad j = 1, \dots, n$$

for any  $k \in \mathbb{N}$ . In other words, the rows of  $\tilde{T}_k = \bar{s} T_k$  vanish in the limit, except for the  $l$ -th and the  $(l+1)$ -th row, which are equal up to a constant factor. Consequently, the scaled homogeneous coordinates  $\tilde{w}_k = \bar{s} w_k = \tilde{T}_k \hat{w}_k$  of  $v$  satisfy

$$\lim_{v \rightarrow \bar{v}} (\tilde{w}_i^k) = 0, \quad i \neq l, l+1$$

and

$$r_l(\bar{v}) \lim_{v \rightarrow \bar{v}} (\tilde{w}_l^k) = r_{l+1}(\bar{v}) \lim_{v \rightarrow \bar{v}} (\tilde{w}_{l+1}^k) > 0, \quad (18)$$

where the last inequality follows from the facts that the circumcentre coordinates  $\hat{w}_k$  of  $\Omega$  are positive for  $k$  sufficiently large and that  $\tilde{T}_k$  is non-negative with strictly positive entries  $\tilde{t}_{l,l}^k$  and  $\tilde{t}_{l+1,l}^k$ , even in the limit. Combining these observations, we have

$$\lim_{v \rightarrow \bar{v}} \lambda_i^k = \lim_{v \rightarrow \bar{v}} \frac{\bar{s} w_i^k}{\sum_{j=1}^n \bar{s} w_j^k} = \lim_{v \rightarrow \bar{v}} \frac{\tilde{w}_i^k}{\sum_{j=1}^n \tilde{w}_j^k} = \lim_{v \rightarrow \bar{v}} \frac{\tilde{w}_i^k}{\tilde{w}_l^k + \tilde{w}_{l+1}^k},$$

hence  $\lim_{v \rightarrow \bar{v}} \lambda_i^k = 0$  for  $i \neq l, l+1$  and, by (18),

$$\lim_{v \rightarrow \bar{v}} \lambda_l^k = \frac{r_{l+1}(\bar{v})}{r_l(\bar{v}) + r_{l+1}(\bar{v})} = 1 - \mu, \quad \lim_{v \rightarrow \bar{v}} \lambda_{l+1}^k = \frac{r_l(\bar{v})}{r_l(\bar{v}) + r_{l+1}(\bar{v})} = \mu,$$

which proves the linear behaviour on the open edge  $(v_l, v_{l+1})$ .

Finally, the *non-negativity* of iterative coordinates follows from Corollary 5, the Lagrange property, and the linearity on the edges.  $\square$

---

**Algorithm 1** Iterative coordinates (with  $O(n \cdot K \cdot \min(n, K))$  time and  $O(n \cdot \min(n, K))$  space complexity)

---

**Input:** planar polygon  $\Omega$  with vertices  $v_1, \dots, v_n$ , point  $v \in \text{int}(\Omega)$ , number of iterations  $K$ **Output:** iterative coordinates  $\lambda_1^K, \dots, \lambda_n^K$  of  $v$  with respect to  $\Omega$ 

```
1: initialize  $W = 0$ ,  $s \in \mathbb{R}^{n+1}$ ,  $w = \mathbf{0} \in \mathbb{R}^n$ ,  $V \in (\mathbb{R}^2)^{n+1}$ , and  $T = \mathbf{0} \in \mathbb{R}^{n \times (n+1)}$ 
2: for  $i = 1$  to  $n$  do ▷ initial projection step
3:    $u := v_i - v$ ,  $r := \|u\|$ ,  $V_i := u/r$ ,  $T_{i,i} := 1/r$  ▷ store  $V_0$  in  $V$  and  $T_0$  in  $T$ 
4:  $V_{n+1} := V_1$ ;  $T_{1,n+1} := T_{1,1}$ 
5: for  $k = 1$  to  $K$  do ▷ perform  $K$  smoothing steps
6:   for  $i = 1$  to  $n$  do ▷ overwrite  $V$  with  $VM S_k$ 
7:      $u := V_i + V_{i+1}$ ,  $s_i := \|u\|$ ,  $V_i := u/s_i$ 
8:      $V_{n+1} := V_1$ 
9:     for  $i = 1$  to  $n$  do ▷ overwrite  $T$  with  $TMS_k$ 
10:      for  $J = n - \min(k, n - 1)$  to  $n$  do
11:        if  $k < n - 1$  then  $j := 1 + (i + J - 1) \bmod n$  else  $j := J$ 
12:           $T_{i,j} := (T_{i,j} + T_{i,j+1})/s_j$ 
13:           $T_{i,n+1} := T_{i,1}$ 
14:      for  $i = 1$  to  $n$  do
15:         $s_i := \det(V_i, V_{i+1}) / (1 + \langle V_i, V_{i+1} \rangle)$  ▷ compute  $\tan(\alpha_i^K/2)$ 
16:         $s_{n+1} := s_1$ 
17:      for  $i = n + 1$  downto  $2$  do ▷ compute circumcentre coordinates  $\hat{w}_K$  of  $\Omega_K$ 
18:         $s_i := s_{i-1} + s_i$  ▷ overwrite  $s_i$  with  $\hat{w}_i^K$ 
19:         $s_1 := s_{n+1}$ 
20:      for  $i = 1$  to  $n$  do ▷ compute homogeneous coordinates  $w_K$  of  $v$ 
21:        for  $J = n - \min(K, n - 1)$  to  $n$  do
22:           $j := 1 + (i + J - 1) \bmod n$ 
23:           $w_i := w_i + T_{i,j} s_j$ 
24:           $W := W + w_i$  ▷ accumulate sum of homogeneous coordinates
25:      for  $i = 1$  to  $n$  do ▷ compute iterative coordinates  $\lambda_1^K, \dots, \lambda_n^K$  of  $v$ 
26:         $w_i := w_i / W$  ▷ overwrite  $w_i$  with  $\lambda_i^K$ 
27: return  $(w_1, \dots, w_n)$ 
```

---

## 5 Implementation

Given a polygon  $\Omega$ , a point  $v \in \text{int}(\Omega)$ , and a number of iterations  $K$ , a straightforward implementation of iterative coordinates can be derived directly from the construction in Section 3.1, as outlined in Algorithm 1. We first compute the matrices  $V_0$  and  $T_0$  (lines 2–4) and then construct the vertices  $V_k$  of the cyclic polygons  $\Omega_k$  as well as the matrices  $T_k$  for  $k = 1, \dots, K$  (lines 5–13) by carrying out the required smoothing and scaling steps as stated in (7) and (9). Note that we always add a copy of the first vertex of  $V_k$  and the first column of  $T_k$  at the end of  $V_k$  and  $T_k$  (lines 4, 8, and 13), so that  $V_{k-1}$  and  $T_{k-1}$  can be overwritten by  $V_k$  and  $T_k$  in each iteration. In the next step, we compute the circumcentre coordinates  $\hat{w}_K$  of  $\Omega_K$  (lines 14–19), up to a factor of 2 that cancels out at the end, using the tangent formula  $\hat{w}_i^K = 2(\tan(\alpha_{i-1}^K/2) + \tan(\alpha_i^K/2))$  and recalling that

$$\tan \frac{\alpha_i^K}{2} = \frac{\sin \alpha_i^K}{1 + \cos \alpha_i^K} = \frac{\det(v_i^K, v_{i+1}^K)}{1 + \langle v_i^K, v_{i+1}^K \rangle}.$$

Finally, we multiply  $\hat{w}_K$  with  $T_K$  to get the homogeneous coordinates  $w_K$  (lines 20–23) and normalize the latter (lines 25–26) to obtain the iterative coordinates  $\lambda_1^K, \dots, \lambda_n^K$  of  $v$  with respect to  $\Omega$ . Note that we exploit the fact that  $T_k$  is a periodic banded matrix with bandwidth  $k + 1$  in lines 10, 11 and 21, 22 to reduce the time complexity of the algorithm from  $O(n^2 K)$  to  $O(nK^2)$  if  $K < n$ . We further optimized Algorithm 1 with respect to memory consumption, so that it gets by with storing only the two vectors  $s \in \mathbb{R}^{n+1}$  and  $w \in \mathbb{R}^n$ , the vector of 2D points  $V \in (\mathbb{R}^2)^{n+1}$ , and the matrix  $T \in \mathbb{R}^{n \times (n+1)}$ . Hence, the space complexity is  $O(n^2)$  and  $O(nK)$  for  $K < n$  if only the non-zero values of  $T$  are stored.

An even more efficient algorithm can be designed (see Algorithm 2) by observing that the vertices  $v_i^K$  of the cyclic polygons  $\Omega_k$  are actually not needed, neither for computing  $\hat{w}_K$ , nor for constructing the matrix  $T_K$ .

---

<sup>1</sup>We wish to thank Sundararajan Natarajan for noticing that this if-statement, which is missing in the published version of this article, is necessary to guarantee that only those  $T_{i,j}$  that are not needed for further computations are overwritten by their new values.

---

**Algorithm 2** Iterative coordinates (with  $O(n \cdot K)$  time and  $O(n \cdot K)$  space complexity)
 

---

**Input:** planar polygon  $\Omega$  with vertices  $v_1, \dots, v_n$ , point  $v \in \text{int}(\Omega)$ , number of iterations  $K$ 
**Output:** iterative coordinates  $\lambda_1^K, \dots, \lambda_n^K$  of  $v$  with respect to  $\Omega$ 

```

1: initialize  $W = 0$ ,  $w \in \mathbb{R}^{n+1}$ ,  $V \in (\mathbb{R}^2)^{n+1}$ , and  $\beta \in \mathbb{R}^{(K+1) \times (n+1)}$ 
2: for  $i = 1$  to  $n$  do                                      $\triangleright$  compute initial shift
3:    $V_i := v_i - v$ 
4:  $V_{n+1} := V_1$ 
5: for  $i = 1$  to  $n$  do                                        $\triangleright$  compute initial angles
6:    $\beta_{0,i} := \text{atan2}(\det(V_i, V_{i+1}), \langle V_i, V_{i+1} \rangle) / 2$   $\triangleright$  store  $\alpha_i^0 / 2$  in  $\beta_{0,i}$ 
7:  $\beta_{0,n+1} := \beta_{0,1}$ 
8: for  $k = 1$  to  $K$  do                                            $\triangleright$  perform  $K$  smoothing steps
9:   for  $i = 1$  to  $n$  do
10:     $\beta_{k,i} := (\beta_{k-1,i} + \beta_{k-1,i+1}) / 2$ 
11:     $\beta_{k,n+1} := \beta_{k,1}$ 
12:   for  $i = 1$  to  $n$  do
13:     $w_i := \tan \beta_{K,i}$                                         $\triangleright$  compute  $\tan(\alpha_i^K / 2)$ 
14:    $w_{n+1} := w_1$ 
15:   for  $i = n + 1$  downto 2 do                                    $\triangleright$  compute circumcentre coordinates  $\hat{w}_K$  of  $\Omega_K$ 
16:     $w_i := w_{i-1} + w_i$                                         $\triangleright$  overwrite  $w_i$  with  $\hat{w}_i^K$ 
17:    $w_1 := w_{n+1}$ 
18:   for  $k = K$  downto 1 do                                        $\triangleright$  compute homogeneous coordinates  $w_K$  of  $v$ 
19:    for  $i = 1$  to  $n$  do                                            $\triangleright$  multiply with  $S_k$ 
20:      $w_i := w_i / \cos \beta_{k-1,i}$ 
21:      $w_{n+1} := w_1$ 
22:    for  $i = n + 1$  downto 2 do                                    $\triangleright$  multiply with  $M$ 
23:      $w_i := w_{i-1} + w_i$ 
24:      $w_1 := w_{n+1}$ 
25:   for  $i = 1$  to  $n$  do                                            $\triangleright$  multiply with  $S_0$ 
26:     $w_i := w_i / \|V_i\|$ 
27:     $W := W + w_i$                                                 $\triangleright$  accumulate sum of homogeneous coordinates
28:   for  $i = 1$  to  $n$  do                                            $\triangleright$  compute iterative coordinates  $\lambda_1^K, \dots, \lambda_n^K$  of  $v$ 
29:     $w_i := w_i / W$                                               $\triangleright$  overwrite  $w_i$  with  $\lambda_i^K$ 
30: return  $(w_1, \dots, w_n)$ 

```

---

Indeed, since  $s_i^k = \|v_i^{k-1} + v_{i+1}^{k-1}\| = 2 \cos \alpha_i^{k-1}$  (see Figure 4) and  $\hat{w}_i^K = 2(\tan(\alpha_{i-1}^K / 2) + \tan(\alpha_i^K / 2))$ , all we need are the angles  $\alpha_i^k$  for  $i = 1, \dots, n$  and  $k = 0, \dots, K$ , or rather the half angles  $\beta_{k,i} = \alpha_i^k / 2$ , which turns out to be even more efficient. For  $k = 0$ , we get these angles directly from the vertices  $v_i$  of  $\Omega$  and the point  $v$  (lines 2–7), and for  $k = 1, \dots, K$ , we use the recurrence relation in (13) (lines 8–11). After computing the circumcentre coordinates  $\hat{w}_K$  of  $\Omega_K$  (lines 12–17), we then determine the homogeneous coordinates  $w_K$  by successively multiplying  $\hat{w}_K$  with  $S_k$  (lines 19–21), up to a factor of 2 that cancels out at the end, and  $M$  (lines 22–24) for  $k = K, K - 1, \dots, 1$  (line 18) and finally by  $S_0$  (lines 25–26), which is correct, because  $T_K = S_0 M S_1 \dots M S_K$ ,

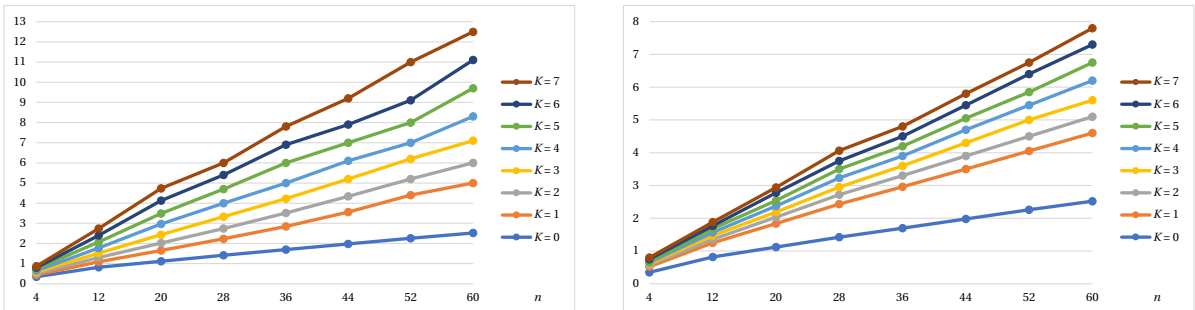


**Figure 9:** Average timings in  $\mu\text{s}$  for computing the mean value coordinates ( $K = 0$ ) of a single point with the algorithm in [12] and its iterative coordinates for  $K = 1, \dots, 7$  using Algorithm 1 (left) and Algorithm 2 (right).

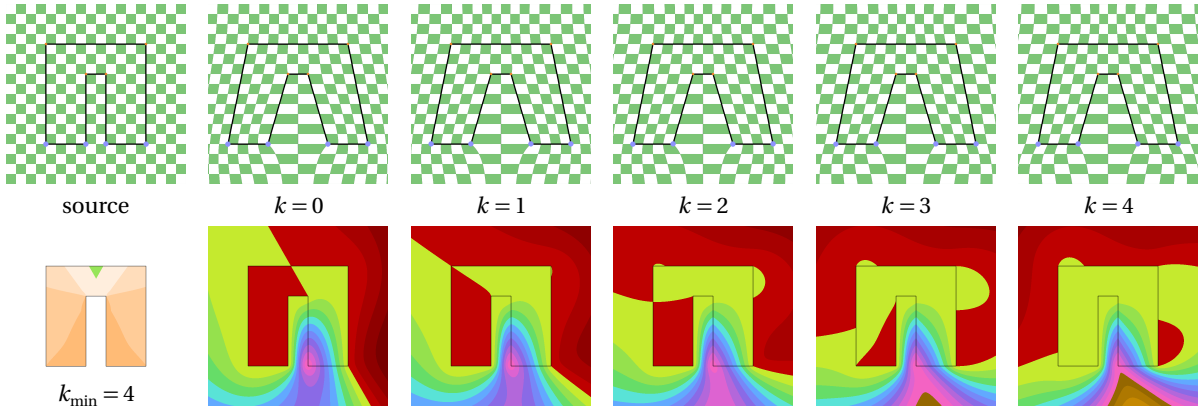


**Figure 10:** Deformation of a source image that is not entirely inside the source control polygon (left), obtained by moving four vertices (blue), using iterative coordinates (top row) and one of the corresponding iterative coordinate functions (bottom row). Function values are visualized using the colour bar in Figure 5.

by (9). The time complexity of this algorithm is only  $O(nK)$ , which clearly beats Algorithm 1, while the space complexity of  $O(nK)$  is the same for  $K \leq n$  and slightly worse for  $K > n$ .

We implemented both algorithms, as well as mean value coordinates, following [12], in *C++* on a Windows 10 laptop with 1.8 GHz Intel Core i7-8565U processor and 16 GB RAM, and the average timings for different values of  $n$  and  $K$  are reported in Figure 9. As expected, Algorithm 2 outperforms Algorithm 1, except for  $k = 1$  and  $n < 40$ , when Algorithm 1 has a slight edge. Compared to mean value coordinates, the computation of iterative coordinates with Algorithm 2 is roughly twice as costly for  $K = 2$  and about three times for  $K = 7$ .

For generating the image deformation examples in Figures 1, 6, and 10, we implemented an interactive application that is based on a GPU version of Algorithm 2. More specifically, we cover the source image with a planar regular quadrilateral mesh  $M$  that has as many vertices as the image has pixels, and then render this mesh as follows. In the vertex shader, we compute for each mesh vertex  $v$  its iterative coordinates  $\lambda_i^K$  with respect to the source control polygon  $\Omega$  and apply them to the vertices of the target control polygon  $\Omega'$ , thus generating the deformed mesh vertex  $v' = \sum_{i=1}^n \lambda_i^K v'_i$ . We then pass  $v'$  as position and the original position  $v$ , scaled to  $[0, 1]^2$ , as texture attribute on to the rasterizer, and the fragment shader simply samples the source image at the interpolated texture coordinates. In this way, the deformed quadrilateral mesh  $M'$  is rendered using the source image as a texture, thus giving the deformed image. Even on a low-end Intel UHD Graphics 620 unit, the application remains interactive up to  $n = 50$  and  $K = 7$  and an image resolution of  $600 \times 600$ , that is, for a mesh with 360 000 vertices.

## 6 Conclusion

Iterative coordinates are a simple, yet powerful and interesting modification of mean value coordinates. On the theoretical side, they are guaranteed to be non-negative and to possess all desired properties of generalized barycentric coordinates after a finite number of iterations. On the practical side, the unwanted effects that are typically caused by negative coordinate values either disappear or fall below a tolerable threshold after few iterations. Hence, they can serve as a valuable extension to any application that is based on mean value coordinates by providing the user with the option to interactively explore the effect of increasing the number of iterations.

### 6.1 Limitations

One feature of mean value coordinates, which distinguishes them from other generalized barycentric coordinates, is that they are also well-defined for points *outside* the polygon  $\Omega$ . To some extent, this property carries over to iterative coordinates and thus allows us to use them for deforming an image, even if it is not entirely contained in the control polygon, as shown in Figure 10. However, while the artefacts due to negative coordinate values still disappear as expected inside the polygon, the deformation result tends to deteriorate outside the polygon.

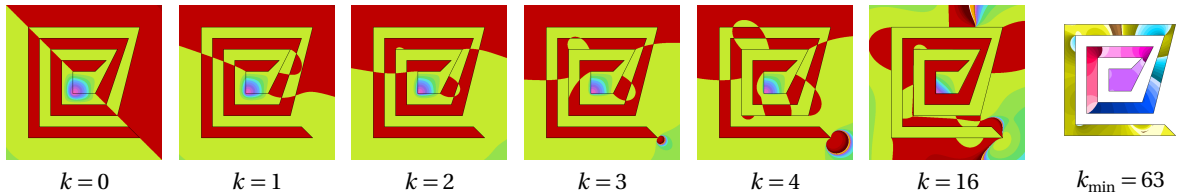


**Figure 11:** Example of an iterative coordinate function with poles occurring outside the polygon (near the bottom right vertex) for  $k \geq 3$  iterations. Inside the polygon, all coordinates are well-defined and non-negative for  $k \geq 63$ . The colour-coding refers to the colour bars in Figures 5 and 7.

Besides this practical shortcoming, points outside  $\Omega$  also have some theoretical issues. On the one hand, Lemma 4 does not extend to the exterior of  $\Omega$ . In fact, if  $v$  is outside  $\Omega$ , then the angles  $\alpha_i^0$  add up to 0 instead of  $2\pi$ , and the polygon  $\Omega_k$  collapses to a single point in the limit. After all, this is not too surprising, since it is clearly impossible for a point outside the convex hull of  $\Omega$  to have only non-negative barycentric coordinates. On the other hand, it may happen that the denominator in (12) vanishes at certain points outside  $\Omega$ , thus leading to undefined coordinate values, although we experienced this only for rather extreme shapes like the “spiral” polygon in Figure 11. Moreover, our experiments indicate that iterative coordinates for  $k \geq 1$ , unlike mean value coordinates, are only  $C^0$  across the edges of  $\Omega$ . Similar problems occur if  $\Omega$  has more than one component or holes, even though mean value coordinates are still well-defined in this case [12]. Overall, we therefore recommend using iterative coordinates only for the interior of a simple polygon  $\Omega$ .

## 6.2 Future work

Regarding the theory of iterative coordinates, we have to admit that so far we did not manage to prove that iterative coordinates are well-defined inside  $\Omega$  for  $k$  smaller than the lower bound in (14). In fact, our current argument for showing that the denominator in (12) does not vanish relies on the positivity of the homogeneous coordinates  $w_i^k$ , which is not necessarily the case for small values of  $k$ . However, we strongly believe that there exists a more refined argument, like the one in [12] for showing the positivity of the denominator for mean value coordinates ( $k = 0$ ) *despite* the potential negativity of some of the  $w_i^k$ , which can be used to prove our conjecture that the denominator in (12) is positive for all  $v \in \text{int}(\Omega)$  and all  $k \in \mathbb{N}_0$ , since this is what we consistently observed in our numerical examples.

An even more desirable result of future work would be an explicit formula or an efficient algorithm for computing the *limit iterative coordinates*  $\lim_{k \rightarrow \infty} \lambda_i^k$ , which are guaranteed to be positive by Lemma 4 and therefore also well-defined, but so far all our attempts to determine this limit were without avail.

Finally, it would be nice to extend the idea of iterative coordinates to polyhedra in 3D. In analogy to our 2D construction, we would project the polyhedron onto the unit sphere around  $v$  and then smooth the resulting spherical polyhedron until it ‘untangles’ and all fold-overs disappear. However, [11] show that the 3D equivalent of our simple midpoint averaging and rescaling procedure is bound to fail, because the spherical polyhedra will not converge to some stable, convex configuration as in 2D, but instead collapse to a single point on the unit sphere. While [11] are able to fix this problem in the context of spherical parameterization by designing a non-linear smoothing operator, it remains unclear how to carry over their non-linear smoothing steps to the level of barycentric coordinates, that is, how to define the non-linear equivalent of our matrices  $T_k$ .

## Acknowledgements

This work was supported by the National Natural Science Foundation of China (NSFC) under the project numbers 61872121 and 61761136010 and the Swiss National Science Foundation (SNSF) under project number 200021-188577.

## References

- [1] D. Anisimov, D. Panozzo, and K. Hormann. [Blended barycentric coordinates](#). *Computer Aided Geometric Design*, 52–53:205–216, Mar.–Apr. 2017. [\[PDF\]](#)
- [2] A. Belyaev. [On transfinite barycentric coordinates](#). In *Proceedings of the Fourth Eurographics Symposium on Geometry Processing*, SGP ’06, pages 89–99, Cagliari, June 2006. Eurographics Association, Aire-la-Ville.

- [3] M. Budninskiy, B. Liu, Y. Tong, and M. Desbrun. [Power coordinates: a geometric construction of barycentric coordinates on convex polytopes](#). *ACM Transactions on Graphics*, 35(6):Article 241, 11 pages, Nov. 2016.
- [4] P. J. Davis. *Circulant Matrices*. Wiley, New York, 1979. ISBN 978-0-471-05771-0.
- [5] M. Eck, T. DeRose, T. Duchamp, H. Hoppe, M. Lounsbery, and W. Stuetzle. [Multiresolution analysis of arbitrary meshes](#). In *Proceedings of the 22nd Annual Conference on Computer Graphics and Interactive Techniques*, SIGGRAPH '95, pages 173–182, Los Angeles, Sept. 1995. ACM, New York.
- [6] A. N. Elmachtoub and C. F. Van Loan. [From random polygon to ellipse: An eigenanalysis](#). *SIAM Review*, 52(1):151–170, Feb. 2010.
- [7] M. S. Floater. [Parametrization and smooth approximation of surface triangulations](#). *Computer Aided Geometric Design*, 14(3):231–250, Apr. 1997.
- [8] M. S. Floater. [Mean value coordinates](#). *Computer Aided Geometric Design*, 20(1):19–27, Mar. 2003.
- [9] M. S. Floater, K. Hormann, and G. Kós. [A general construction of barycentric coordinates over convex polygons](#). *Advances in Computational Mathematics*, 24(1–4):311–331, Jan. 2006. [PDF]
- [10] A. Gillette, A. Rand, and C. Bajaj. [Constructions of scalar and vector finite element families on polygonal and polyhedral meshes](#). *Computer Methods in Applied Mechanics and Engineering*, 16(4):667–683, Oct. 2016.
- [11] C. Gotsman, X. Gu, and A. Sheffer. [Fundamentals of spherical parameterization for 3D meshes](#). *ACM Transactions on Graphics*, 22(3):358–363, July 2003.
- [12] K. Hormann and M. S. Floater. [Mean value coordinates for arbitrary planar polygons](#). *ACM Transactions on Graphics*, 25(4):1424–1441, Oct. 2006. [PDF]
- [13] K. Hormann and N. Sukumar. [Maximum entropy coordinates for arbitrary polytopes](#). *Computer Graphics Forum*, 27(5):1513–1520, July 2008. [PDF]
- [14] K. Hormann and N. Sukumar, editors. [Generalized Barycentric Coordinates in Computer Graphics and Computational Mechanics](#). Taylor & Francis, CRC Press, Boca Raton, 2017. ISBN 978-1-4987-6359-2.
- [15] P. Joshi, M. Meyer, T. DeRose, B. Green, and T. Sanocki. [Harmonic coordinates for character articulation](#). *ACM Transactions on Graphics*, 26(3):Article 71, 9 pages, July 2007.
- [16] T. Ju, S. Schaefer, and J. Warren. [Mean value coordinates for closed triangular meshes](#). *ACM Transactions on Graphics*, 24(3):561–566, July 2005.
- [17] J. A. Kalman. [Continuity and convexity of projections and barycentric coordinates in convex polyhedra](#). *Pacific Journal of Mathematics*, 11(3):1017–1022, Fall 1961.
- [18] X.-Y. Li and S.-M. Hu. [Poisson coordinates](#). *IEEE Transactions on Visualization and Computer Graphics*, 19(2):344–352, Feb. 2013.
- [19] Y. Lipman, J. Kopf, D. Cohen-Or, and D. Levin. [GPU-assisted positive mean value coordinates for mesh deformations](#). In *Proceedings of the Fifth Eurographics Symposium on Geometry Processing*, SGP '07, pages 117–123, Barcelona, July 2007. Eurographics Association, Aire-la-Ville.
- [20] C. T. Loop and T. D. DeRose. [A multisided generalization of Bézier surfaces](#). *ACM Transactions on Graphics*, 8(3):204–234, July 1989.
- [21] E. A. Malsch, J. J. Lin, and G. Dasgupta. [Smooth two dimensional interpolants: A recipe for all polygons](#). *Journal of Graphics Tools*, 10(2):27–39, 2005.
- [22] J. Manson, K. Li, and S. Schaefer. [Positive Gordon–Wixom coordinates](#). *Computer-Aided Design*, 43(11):1422–1426, Nov. 2011.
- [23] M. Meyer, A. Barr, H. Lee, and M. Desbrun. [Generalized barycentric coordinates on irregular polygons](#). *Journal of Graphics Tools*, 7(1):13–22, 2002.
- [24] A. F. Möbius. [Der barycentrische Calcul](#). Johann Ambrosius Barth, Leipzig, 1827.
- [25] J. Tao, B. Deng, and J. Zhang. [A fast numerical solver for local barycentric coordinates](#). *Computer Aided Geometric Design*, 70:46–58, Mar. 2019.
- [26] E. L. Wachspress. *A Rational Finite Element Basis*, volume 114 of *Mathematics in Science and Engineering*. Academic Press, New York, 1975. ISBN 978-0-12-728950-2.
- [27] J. Warren. [Barycentric coordinates for convex polytopes](#). *Advances in Computational Mathematics*, 6(1):97–108, Dec. 1996.
- [28] J. Warren, S. Schaefer, A. N. Hirani, and M. Desbrun. [Barycentric coordinates for convex sets](#). *Advances in Computational Mathematics*, 27(3):319–338, Oct. 2007.
- [29] J. Zhang, B. Deng, Z. Liu, G. Patané, S. Bouaziz, K. Hormann, and L. Liu. [Local barycentric coordinates](#). *ACM Transactions on Graphics*, 33(6):Article 188, 12 pages, Nov. 2014. [PDF]